AUT Journal of Civil Engineering

AUT J. Civil Eng., 5(2) (2021) 325-338
DOI: 10.22060/ajce.2021.19849.5750

Seismic Evaluation of Coupled Shear Walls with Divided Coupling Beams

A. Gholizad* , S. Teymour-Moghaddam, V. Akrami

Faculty of Engineering, University of Mohaghegh Ardabili, Ardabil, Iran.

ABSTRACT: Coupling beams of a coupled shear wall system play an important role in the overall behavior of the structure. Due to the nature of coupling beams, which are mostly sections with high depth and short length, these components are classified as deep beams. A large amount of internal shear force in these beams causes shear-slip across the beam-wall interface which is a brittle break-out. Any increase in ductility of coupling beams will improve the overall performance of the structure against lateral loads. In this regard, the effects of changing the failure mode into flexural mode are investigated by dividing the deep connector beams into two separate beams. As in the divided beams, more internal forces will be delivered by the longitudinal reinforcement bars, it is expected that the shear walls connected with these flexural connectors represent more ductile behavior. To examine this idea, the coupled shear wall system is modeled numerically and its behavior under cyclic loading is verified against experimental data. Five- and eight-story coupled shear walls with coupling beams of different height and reinforcement ratios are modeled and studied. The results show that if the shear and bending strength of divided coupling beams are proportioned properly, they will act in a flexural mode without having an adverse effect on the overall strength of the entire coupled wall.

Review History:

Received: Apr. 11, 2021
Revised: Oct. 19, 2021
Accepted: Nov. 06, 2021
Available Online: Nov. 15, 2021

Keywords:

Coupled shear walls
Divided coupling beam
Cyclic loading
Failure mechanism
Energy dissipation.

1- Introduction

Coupled shear walls consisting of coupling beams and wall piers are widely used as lateral load resisting systems in modern structures [1]. This structural system offers distinct advantages such as good displacement control, the possibility of using slender walls without violating drift limits, and larger hysteretic damping than any other conventionally constructed reinforced concrete (RC) system [2]. Initial research in this area was focused on providing methods for analyzing this structural system [3-5]. With improved engineering understanding towards this structural system, extensive research was carried out on different characteristics of the coupled shear walls such as the effect of degree of coupling (DOC) between wall piers, coupling beam reinforcement layout, etc. [2, 6, 7]. In addition to studies that focus on the overall behavior of the coupled shear walls, other studies have also been conducted on the behavior of coupling beams [1, 8-14]. According to past research, coupling beams are expected to endure significant inelastic deformations under design-level earthquakes and thus, should have appropriate ductility and energy dissipation capacity [11]. Basically, the reinforced concrete beams fail either in flexural or shear mode. The shear mode of failure in these beams is undesired mainly being a brittle failure [11, 15-18].

In the past years, some researchers have focused on changing the behavior of coupling beams from shear mode into flexural action to prevent premature brittle failure of these central components [19, 20]. This can be done by decreasing the depth of coupling beams which may have an adverse effect on the overall strength of entire the shear wall. A solution to this problem is to use two shallow coupling beams at each story separated by a small gap between them [19, 21]. Most of the references addressing this issue deal with the experimental investigation of such components [19, 22, 23] or numerical modeling of coupling beams solely (not in the frame scale) [24-28]. To the best of the authors' knowledge, the only existing study in this field that addresses the finite element modeling of entire coupled shear wall system with dual coupling beams is conducted by Yu *et al.* [29] (in Chinese). They have analyzed a four-story coupled shear wall under cyclic loading and compared the results to the one obtained from analyzing the same coupled shear wall with dual coupling beams. Apart from the limited number of models, the cyclic load-displacement curves presented for analyzed models suggest that the cracking behavior of the concrete material is not considered in the modeling. In line with this trend, the current study aims at evaluating seismic performance of coupled shear walls with divided coupling beams. The parameters, assumptions, modeling techniques and obtained results are discussed in the following sections.

*Corresponding author's email: gholizad@uma.ac.ir

Copyrights for this article are retained by the author(s) with publishing rights granted to Amirkabir University Press. The content of this article is subject to the terms and conditions of the Creative Commons Attribution 4.0 International (CC-BY-NC 4.0) License. For more information, please visit https://www.creativecommons.org/licenses/by-nc/4.0/legalcode.

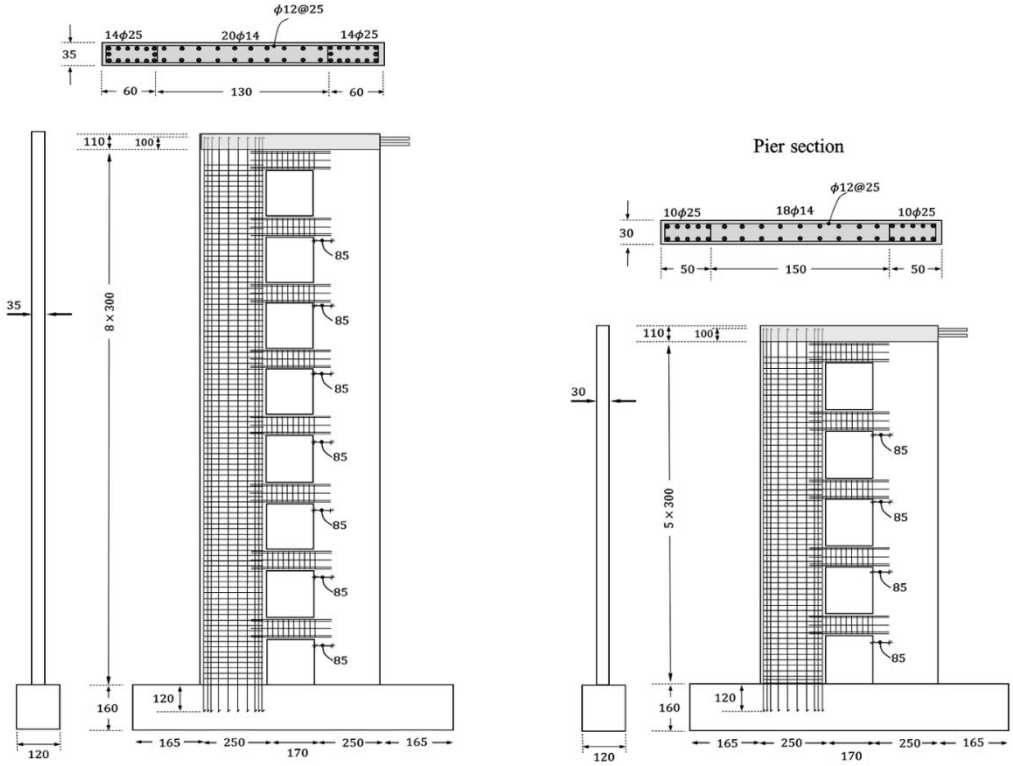

Fig. 1. Geometry and parameters of 5 & 8 story coupled shear walls (unit: cm).

2- Characterization of Failure Mechanism

Since the common coupling beams have very small span/depth ratios, the dominant failure mode in these beams is a shear fracture. The purpose of splitting a deep coupling beam into two shallower superseding beams is to change the failure mechanism of these components from shear to bending which is characterized by the formation of flexural plastic hinges at two ends of the beam. These beams must be designed in such a way that they provide adequate strength equal to the original beam. On the other hand, to ensure that the beam behaves in the flexural mode, the amount of bending and shear strength of these beams should be proportioned carefully. To have divided beams with the same strength as the original coupling beam, the required shear strength in secondary beams, V_u', should be greater than half the shear capacity of the original coupling beam, $½V_r$. On the other hand, as it is intended to have a flexural failure mechanism in divided coupling beams, the ultimate shear force in these beams will be equal to $V_u'=2M_r'/l$, where, M_r' is the flexural strength of secondary beams in divided configuration and, l, is the distance between two piers. Therefore, the flexural strength of secondary beams, M_r', should be greater than $¼V_r.l$. This criterion assures that the divided coupling beam has the same strength as the original one. However, to ensure that the coupling beam behaves in the flexural mode, the shear force corresponding to the flexural failure of divided beams (i.e., $V_u'=2M_r'/l$) should be less than the shear capacity of the original beam, V_r'. Combining these two criteria, one can obtain a relation between shear and flexural strength of divided coupling beams:

$$\frac{V_r.l}{4} \le M_r' \le \frac{V_r'.l}{2} \quad (1)$$

The first criterion assures that the overall strength of two replacement beams will be equal to the original undivided beam and the second criterion guarantees that the divided beams will behave in flexural mode. The larger the range between these two bounds, the easier the selection of bending capacity and the greater the confidence about the flexural behavior of the divided beams. Considering that the shear capacity of beams is directly related to the height of the section, it is expected to have a wider range for bending capacity of divided beams by increasing their height.

3- Details of Numerical Models

3- 1- Geometry of models

Twenty-six coupled shear walls with different numbers of stories, coupling beams, and reinforcement ratios are modeled and studied in this paper. The analyzed models can be classified into two categories based on their total height. The first category includes shear walls from a low-rise structure comprising five stories whereas the second one includes models corresponding to an eight-story mid-rise building (Fig. 1).

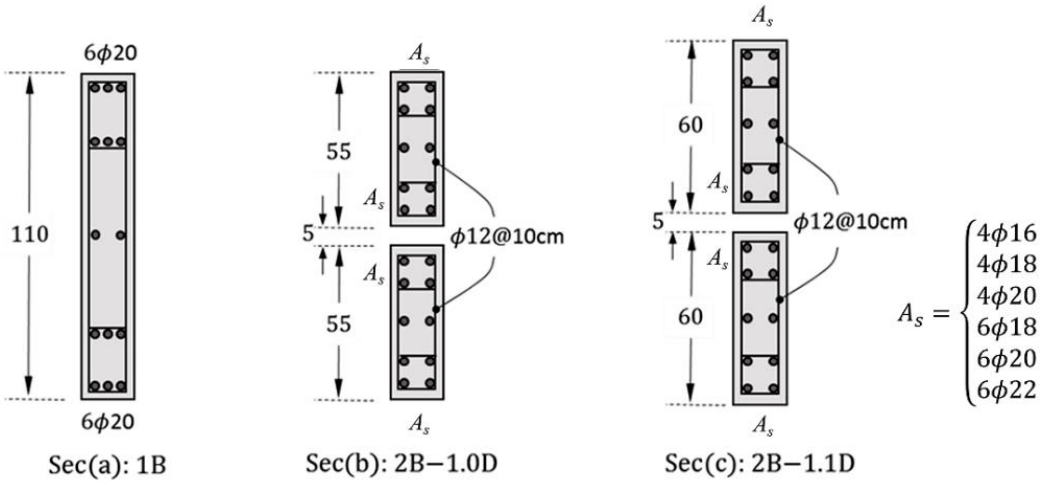

Fig. 2. Geometry and parameters of coupling beams.

Inside each category, there are three types of models with different coupling beams (Fig. 2). The first type is representative of traditional coupled shear walls in which the piers are tied using a single coupling beam at the level of each story (1B model).

Values obtained from the analysis of this type are used as the reference points to address the results of the other models. The other two types are the same as the first one except that the coupling beams are divided into two separate beams and a 50 mm gap is provided between the two parts (see Fig. 2). For the second type, the total height of resultant beams equals the depth of the original beam (2B-1.0D models), while for the third type the total height of beams is 10% greater than the original depth (2B-1.1D models). For all models, the story height is assumed to be 3000 mm. Dimensions of the piers and coupling beams are selected so that the coupling beams contribute mainly to the overall behavior of the entire shear wall. Accordingly, the width of the piers is assumed to be 2500 mm. Also, knowing that the appropriate height for coupling beams is about 30% of the story height, the depth of the coupling beams for the reference wall (1B model) is assumed to be 1100 mm. Reinforcement of the piers and coupling beams are calculated as per ACI 318 [30]. The compressive strength of the concrete and the yield stress of the reinforcement bars are assumed to be 30 and 300 MPa, respectively.

3- 2- Finite element modeling

Finite element modeling and analysis of the specimens are conducted using LS DYNA software. The smeared crack Winfrith model (MAT085) [31, 32] has been used for the modeling of concrete. It assumes elastic-perfectly plastic behavior in compression and its yield surface expands as the hydrostatic pressure increases [33]. The radii at the compressive and tensile meridian are determined using the compressive and tensile strengths of concrete [31]. This material model provides additional information on crack locations, directions, and widths [34, 35]. The reinforcing bars are modeled with an isotropic-kinematic hardening plasticity model (MAT003) [34, 35] used for steel material. Also, the interaction between concrete and steel reinforcement is simulated using Constrained-Lagrange-in-Solid (CLS) formulation [34, 35]. This interaction causes coupling between steel and concrete materials and thus, the degrees of freedom for each node of reinforcement elements are calculated using the degrees of freedom of concrete elements adjacent to this node (Fig. 3).

As the selected model for concrete material (MAT085) can be only implemented in the 8 node single integration point continuum elements, three-dimensional cube elements with reduced integration have been used for modeling concrete. A mesh sensitivity analysis was conducted to see the effect of mesh size on the results of numerical analysis. Two meshing schemes were considered. The first and second schemes had 6 & 12 divisions along the width of piers, 4 & 8 divisions along the length of beams, and 3 & 5 divisions along with the beam height, respectively. Comparison of load-displacement curves for two models showed a maximum difference being less than 2% while the adoption of the second meshing scheme increased the CPU time by a factor of 2.5. The number of divisions for the main models is selected between two studied meshing schemes (i.e., 9 divisions for the width of piers, 6 divisions for the length of beams, and 4 divisions along with the depth of beams). For modeling steel reinforcement, truss elements with 2 nodes have been used.

3- 3- Constraints and loading

The effect of the base support is simulated using zero displacement constraint at the bottom of the concrete foundation. Also, an additional constraint is specified to restrict the out-of-plane deformation of the specimen. This constraint has been applied to the lateral surface of the wall piers. The gravity loading on each pier has been calculated as the cross-section area of the pier multiplied by 10% of the specified concrete strength and applied at the top of the piers. The lateral loading sequence is controlled by roof drift angle, be-

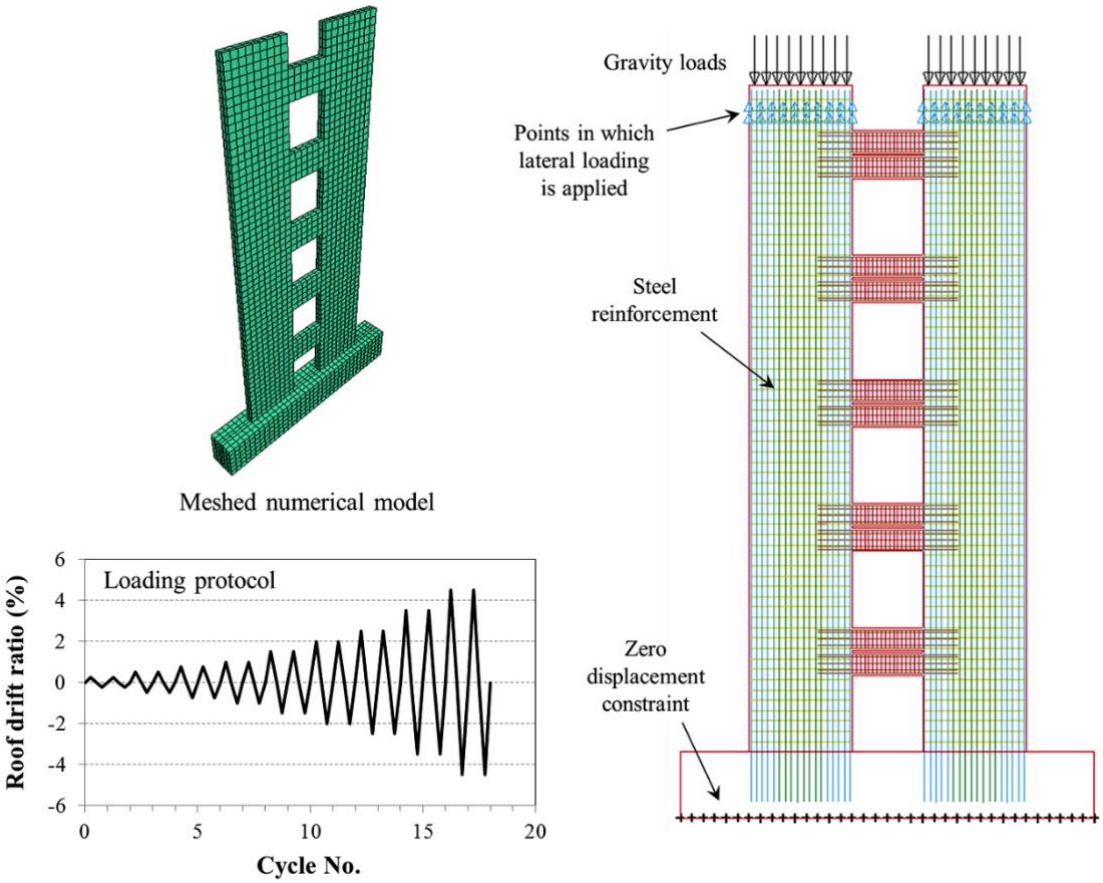

Fig. 3. Finite element modeling, constraints, and loading.

ginning with four increments of 0.25% drift, with two cycles of loading at each step. The next three steps are increasing at 0.5% drift, followed by two steps of loading increasing at 1.0% drift. The loading protocol was the same as the one used by Aejaz and Wight [36] in their experiments.

3- 4- . Verification of models

Modeling techniques adopted in the current study are verified using the results of the experimental study conducted by Lu and Chen [37]. This research reports the results of cyclic loading on three coupled shear walls. The specimen "CW-2" is used for verification purposes. The selected specimen (shown in Fig. 4(a)), is modeled using the mechanical properties reported in the corresponding reference and subjected to the same loading history as that applied to the specimens during the laboratory test. As the tested specimen had a displacement sensor at the base, the base of the specimens was assumed to be fixed with zero displacements. For the selected specimen, the loading had been applied at the top of the shear wall. Fig. 4(b) shows the crack pattern at the bottom of the wall piers which suggests that both numerical and experimental specimens underwent almost the same procedure of cracking. In addition, hysteresis loops obtained from FE analysis and laboratory test are plotted in Fig. 4(c) according to which it can be seen that the curves for both cases match well.

4- Parametric Study

4- 1- Load-displacement behavior

The numerical models were subjected to cyclic loading and the total base shear was plotted versus the roof displacement. Fig. 5 shows the hysteretic curves of 5 and 8-story models with a single coupling beam. The figure also represents the distribution of Von-mises stresses at a 1.5% drift angle according to which, it can be seen that the connected piers act together to withstand the applied lateral load. As mentioned before, the results of these two models are used as the benchmark to address the results of the other models.

Fig. 6 displays load-displacement curves for coupled shear walls with divided beams. The vertical axis of these plots is normalized using the maximum lateral load resisted by the corresponding reference model. The first and second columns contain graphs for 5 story walls with "2B-1.0D" and "2B-1.1D" beams while the third and fourth columns represent the same graphs for 8 story models. The graphs of each row represent the behavior of the models with the coupling beam having a certain amount of longitudinal reinforcement. The summary of these graphs is also presented in Table 1. Based on the results of "2B-1.0D" models with the same reinforcement ratio (see Table 1), it can be seen that the maximum load-carrying capacity of these models is less than the ultimate strength of the corresponding reference model.

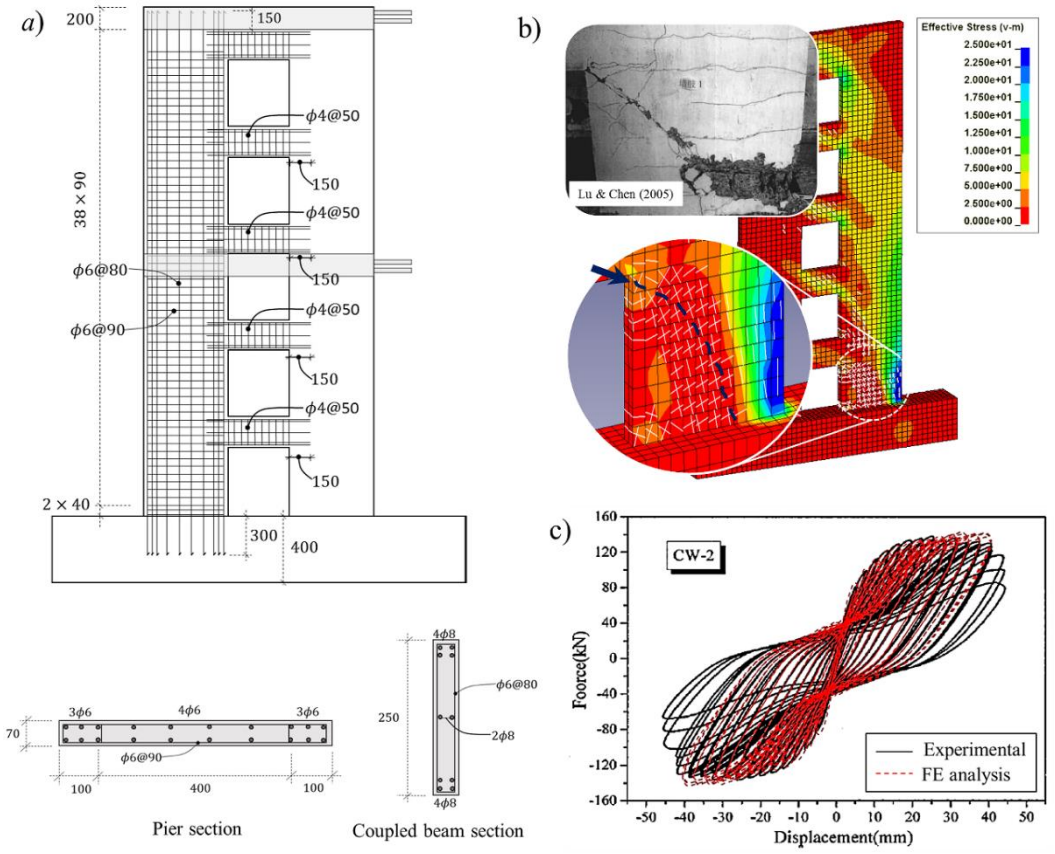

Fig. 4. Verification of FE modeling using the experimental data reported by Lu and Chen (2005); a) details of the reference model; b) crack pattern; c) load-displacement curves.

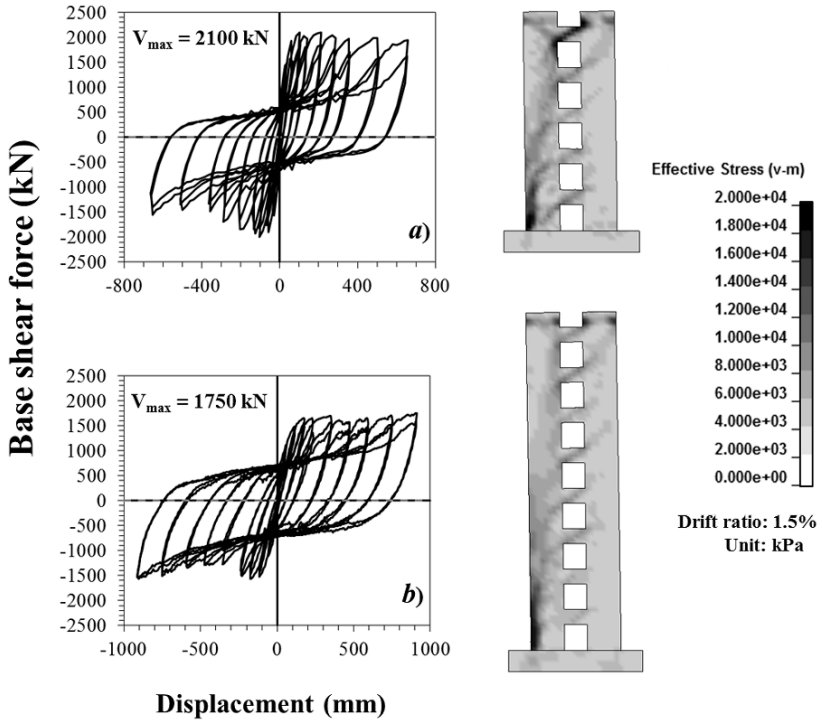

Fig. 5. Load-displacement curves for 5 & 8 story models with single coupling beam.

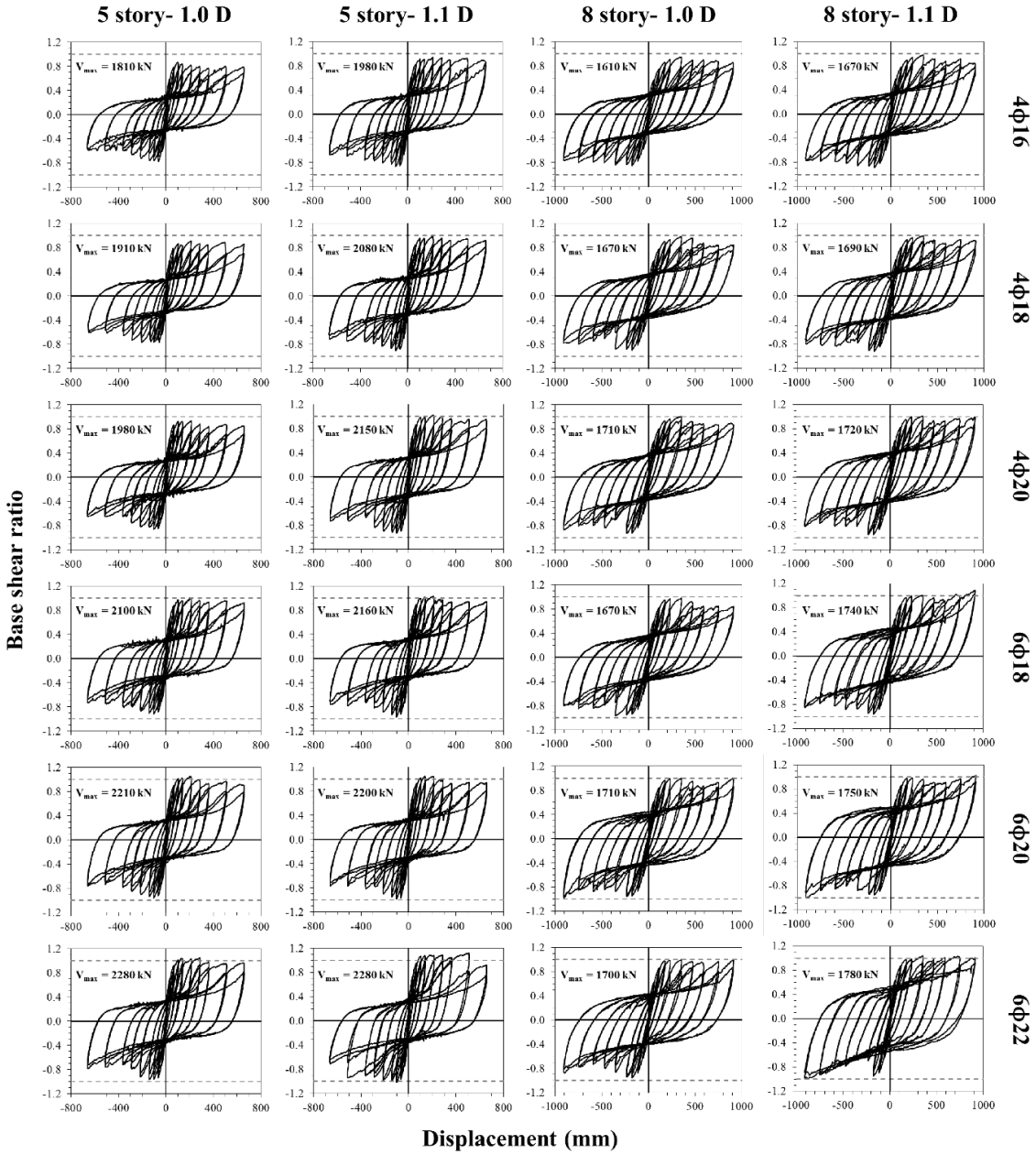

Fig. 6. Load-displacement curves for coupled shear walls with divided beams.

However, as the reinforcement ratio of coupling beams increases the strength of coupled walls becomes equal to or even greater than the ultimate bearing capacity of the reference model. Referring to the results of the "2B-1.1D" models, it can be seen that when the total height of divided beams increases by 10%, the coupled shear walls can achieve the ultimate capacity of the reference model even with the same reinforcement ratio. Again, as the reinforcement ratio of coupling beams increases, the strength of coupled walls becomes more and more.

4- 2- Envelope backbone curves

Backbone curves for analyzed models were constructed as the envelope of cyclic curves and presented in Fig. 7. Also, the initial stiffness of the models was calculated based on the provided envelope backbone curves (i.e., Fig. 7) and summarized in Table 1. According to the table, the maximum reduction in initial stiffness of the models corresponds to the 5-story shear wall with the weakest coupling beam. This is due to the reduction in flexural stiffness of the coupling beams caused by diving them into two beams.

Given that none of the samples has a resistance reduction of more than 25% within the considered drift range, no information can be provided about the maximum displacement capacity or ductility of the specimens. However, it can be said that the ductility ratio (maximum displacement capacity divided by yield displacement) for 5 and 8 story models is more than nearly 6.0 and 5.0, respectively.

Table 1. Summary of results for 5 and 8-story models.

Beam type	Reinforcement		Type of Plastic region	Comparison to the reference model				
	No.	ratio		Reinforcement ratio	Capacity ratio		Stiffness ratio	
					5 story	8 story	5 story	8 story
2B-1.0D	4ϕ16	0.0048	Flexural	0.85	0.86	0.95	0.88	0.91
	4ϕ18	0.0062	Flexural	1.08	0.91	0.98	0.88	0.93
	4ϕ20	0.0076	Flexural	1.33	0.93	1.00	0.88	0.95
	6ϕ18	0.00923	Flexural	1.61	1.00	1.00	0.92	0.96
	6ϕ20	0.011	Transitional	2.00	1.04	1.00	0.94	0.98
	6ϕ22	0.014	Shear	2.42	1.05	1.00	0.94	0.99
2B-1.1D	4ϕ16	0.0044	Flexural	0.85	0.94	0.98	0.89	0.94
	4ϕ18	0.0056	Flexural	1.08	1.00	0.99	0.92	0.97
	4ϕ20	0.0069	Flexural	1.33	1.03	1.01	0.97	0.98
	6ϕ18	0.0085	Flexural	1.61	1.03	1.02	0.97	1.01
	6ϕ20	0.0104	Transitional	2.00	1.05	1.03	0.97	1.01
	6ϕ22	0.0126	Shear	2.42	1.09	1.05	0.98	1.01

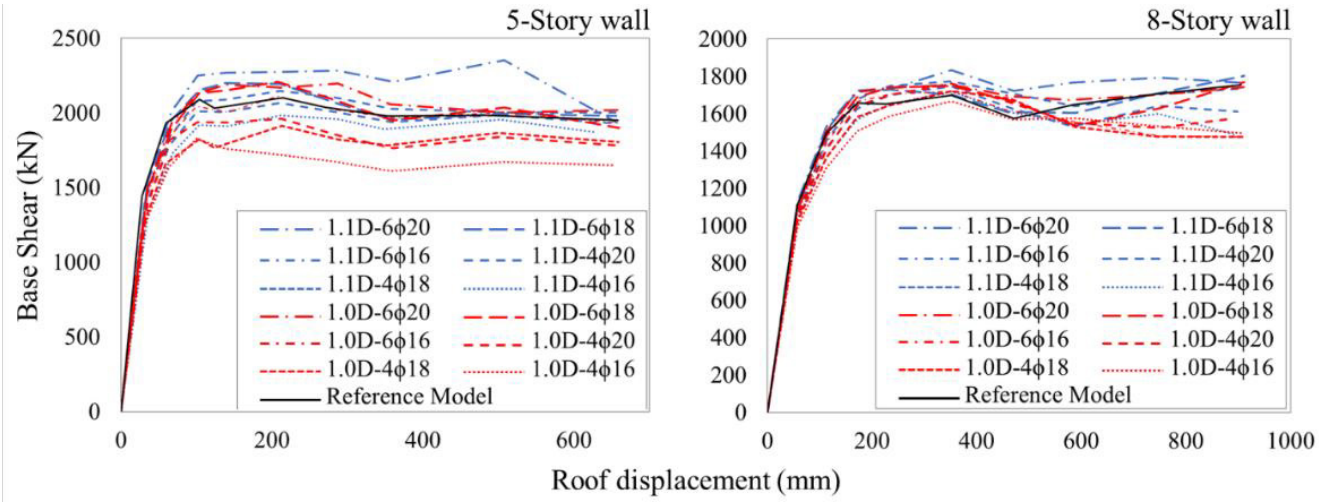

Fig. 7. Backbone curves for analyzed models constructed as the envelope of cyclic data.

4- 3- Failure mechanisms of the models

The yield pattern of coupling beams at the third story of the models is depicted in Fig. 8. Based on these patterns, the type of plastic region associated with each model is characterized and summarized in Table 1. According to the figure, the failure of coupling beams in reference models is due to the formation of the shear plastic region. However, as the coupling beam is divided into two parts, different failure mechanisms are observed depending on the amount of longitudinal reinforcement. For divided beams with the least amount of reinforcement, the dominant failure mechanism is flexural yielding, characterized by localized plastic areas at the ends of the beams. According to Table 1, the ultimate load-carrying capacity of these models is less than the corresponding reference models. This clearly shows the effect of neglecting the first criterion given in Eq. (1). As the reinforcement ratio of coupling beams increases the overall strength of models increases too. This increase continues until for a specific reinforcement ratio the strength of the model reaches the ultimate bearing capacity of the reference model (acceptable range). This manner keeps on until the further increase of the longitudinal reinforcement causes the violation of the second criterion in Eq. (1) which means that the coupling beam will fail in shear mode.

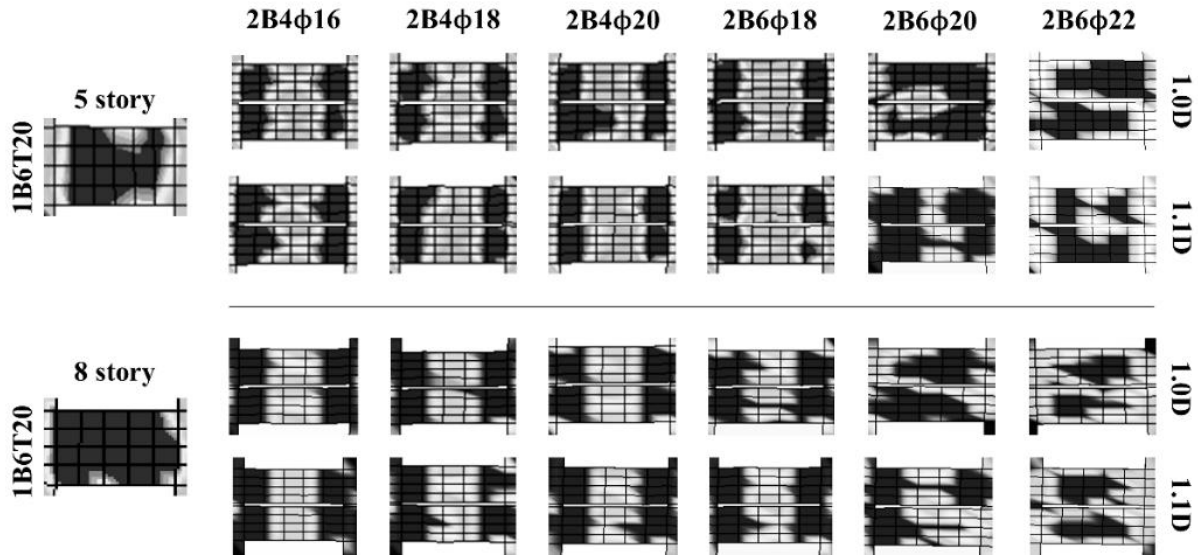

Fig. 8. Yield pattern of coupling beams at the last cycle of loading.

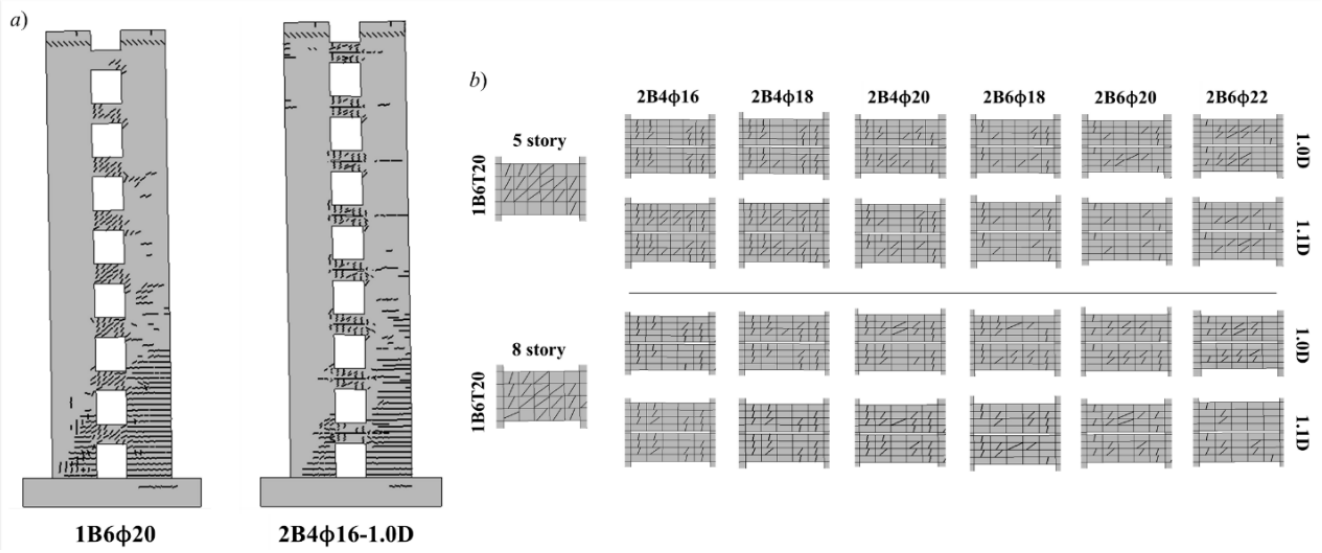

Fig. 9. Cracking pattern for models with single and divided beams; a) piers (1.5% drift); b) coupling beams (0.5% drift).

4- 4- Cracking pattern

As mentioned before, the adopted smeared crack Winfrith model can provide additional information on crack locations, directions, and widths. This information can be used to gain a better understanding of the behavior of the models. Fig. 9(a) displays the cracking pattern of two eight-story models with single and divided coupling beams at a 1.5% drift ratio. Cracks with a width greater than 5 mm are shown in the figure.

An important issue to be addressed in this figure is the propagation of vertical cracks at the bottom of the compression pier in the reference model which cannot be seen in the model with divided beams. Another difference is the shear cracking of the wall piers along the gap provided between two beams in the proposed double beam model. Finally, the cracking pattern of coupling beams can be compared to each other according to which it can be seen that the propagation of cracks in divided beams is more like flexural cracking. According to Fig. 9(b), as the number of longitudinal reinforcement increases, the cracking pattern changes from vertical cracking at the ends of the beams to the inclined cracking at the center of beams.

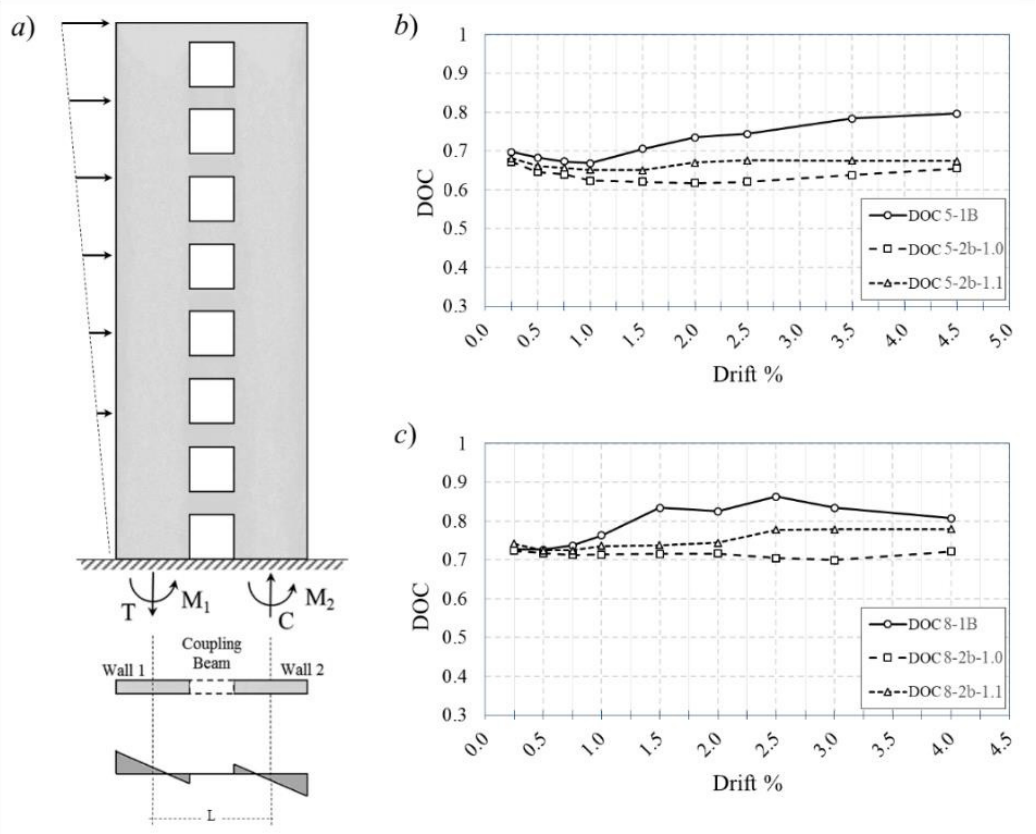

Fig. 10. Comparison of the degree of coupling; a) axial forces and bending moments at the base of wall piers; b) DOC for 5-story walls c) DOC for 8-story walls.

4- 5- Degree of coupling

The degree of coupling is a measure to determine how much the coupled shear wall system acts as an integrated Lateral load resisting system or in contrast, as two individual shear walls. For a given coupled shear wall system, this measure can be calculated from the following expression [38]:

$$DOC = \frac{T.L}{\sum M_w + T.L} \quad (2)$$

Where T is the axial force in each pier, L is the center to center distance of piers, $T.L$ is the moment due to integrated action of piers, and M_w is the bending moment at the base of each shear wall (see Fig. 10a). The DOC for studied shear wall systems is calculated at each drift ratio and is plotted in Figs. 10(b) and 10(c) for five and eight-story models, respectively. Each graph contains two curves for shear walls having "2B-1.0D" and "2B-1.1D" beams with 6ϕ18 longitudinal reinforcements along with the curve corresponding to the reference model with single coupling beams at each level.

As it can be seen in the graphs, the models with divided and undivided coupling beams have nearly the same DOC at the beginning of the loading. According to the figure, there is almost the same pattern in all curves for the rest of loading starting with an initial decrease of DOC followed by its increase at higher drift ratios. With a closer look at Eq. (2), one can see that the increase of DOC can conclude from a decrease of M_w which means degradation of wall piers (the statement is checked by investigating FE models). On the contrary, the decrease of DOC can result from a decrease of $T.L$ which is a sign of degradation in coupling beams. With this interpretation, it can be seen that the degradation of wall piers in models with divided coupling beams starts at higher drift ratios, compared to reference models.

4- 6- Energy dissipation

To compare the energy dissipated by different models, it is important to first introduce a damage indicator in numerical models. For this purpose, the excessive decrease of stiffness in one of the structural floors accompanied by a sudden increase in inter-story drift is considered as the criterion to cut the cyclic curve. Fig. 11 displays graphs of story shear against inter-story drift ratio at different stories of the 5 story reference model. Graphs in each row correspond to a specific roof drift angle mentioned at the end of the row. According to the graphs of the first row which correspond to the total drift of 1%, it can be seen that the distribution of inter-story drift ratio is almost uniform along the height of the model and all

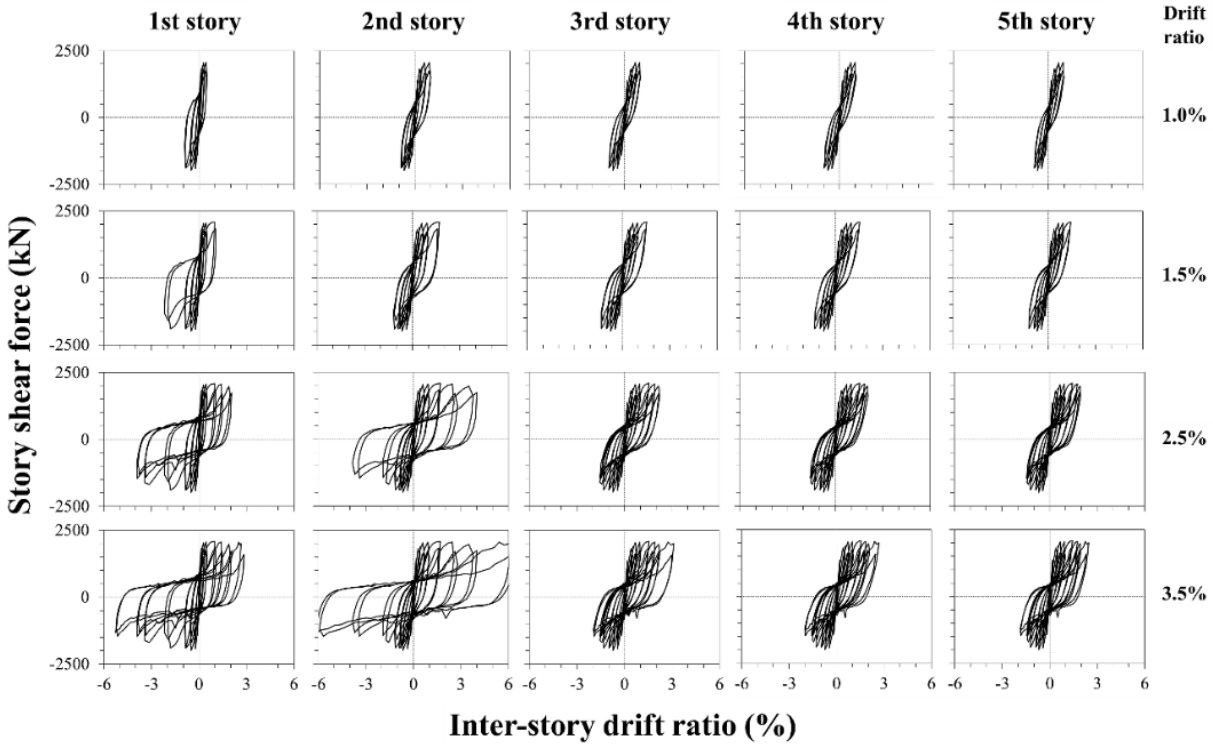

Fig. 11. Graphs of story shear vs. inter-story drift ratio for 5 story reference model.

stories have nearly the same contribution to the total energy dissipation of the system. However, as the total displacement at the roof level increases, the first and second stories experience an extra increase in inter-story drift ratio compared to other stories. Focusing on the graphs of the last row it can be seen that although the global drift ratio at the roof level is 3.5%, the second story has experienced more than a 6% inter-story drift ratio. Graphs of Fig. 11 are summarized in Fig. 12

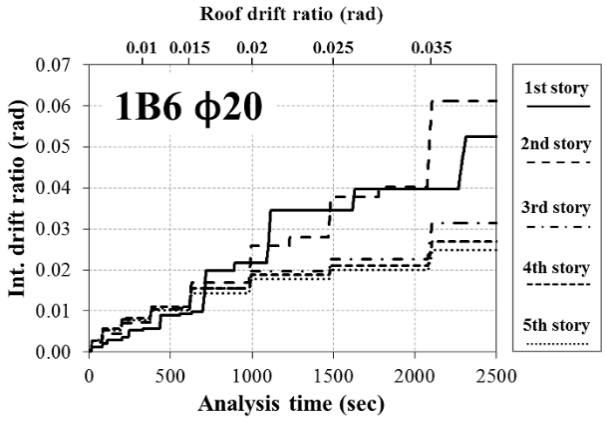

Fig. 12. Growth of drift ratio at different stories of 5 story reference model during the cyclic loading.

which displays the growth of maximum drift ratio at different stories of 5 story reference model during the cyclic loading. The same plots for the other 5 story models are depicted in Fig. 13. Looking at the first graph (least reinforcement ratio) it can be seen that the distribution of inter-story drift ratio for this model is almost uniform.

The maximum inter-story drift ratio is 4% as per the 3.5% global drift ratio. However, as the amount of longitudinal reinforcement in coupling beams increases (behavior changes to shear mode) the non-uniformity of inter-story drift becomes more intense and starts in lower drift ratios. The results presented in the last graph which correspond to the model with maximum reinforcement ratio are analogous to the curves obtained for the reference model (Fig. 12). Specifying the amount of drift ratio at which the sudden loss of stiffness begins to occur in the most critical story, the dissipated cumulative hysteretic energy is calculated for different models and plotted in Fig. 14.

According to the figure, for all five-story models, the energy dissipation of specimens with divided coupling beams is equal to or greater than the value corresponding to the reference model. As the flexural reinforcement ratio in coupling beams increases, the energy dissipation increases until the model "2B4ϕ18" attain the highest energy dissipation. The hysteretic energy dissipated by this model is approximately 2.5 times the energy dissipated by the reference model. The further increase of reinforcement ratio causes the decrease of cumulative hysteretic energy dissipation.

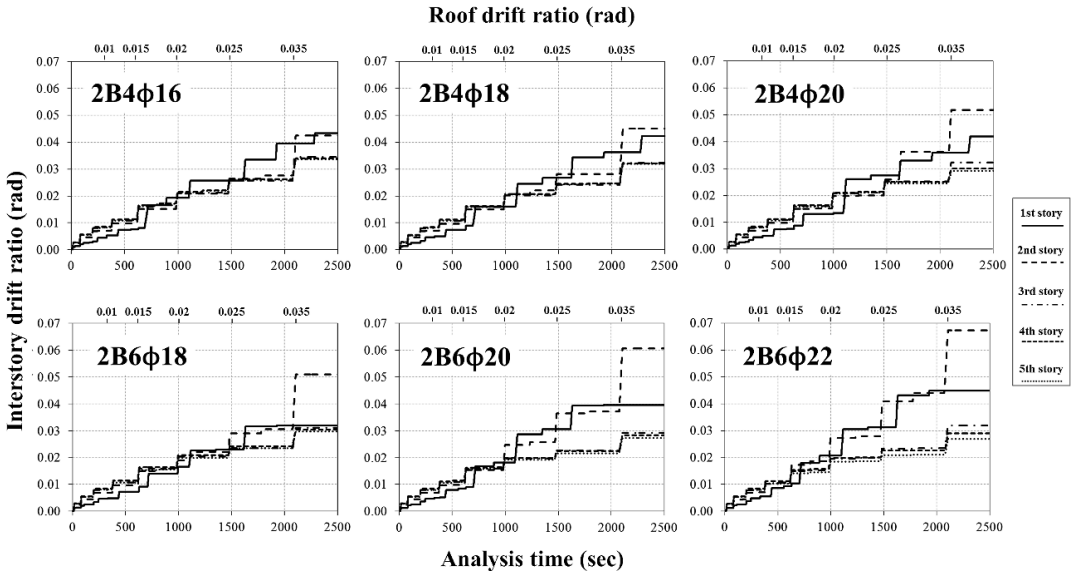

Fig. 13. Comparing the distribution of inter-story drift ratio for 5 story models with 1.1D.

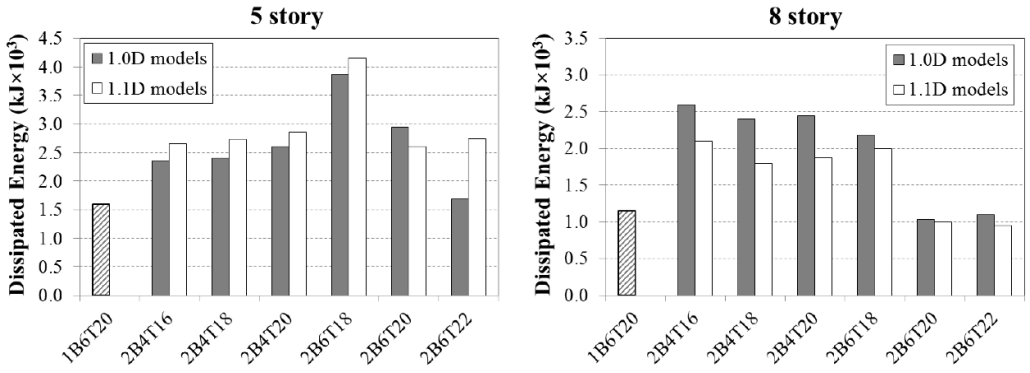

Fig. 14. Comparing cumulative hysteretic energy dissipation for analyzed models.

For eight-story models, it can be seen that the specimens with flexural coupling beams have higher energy dissipation compared to the reference model. The energy dissipated by these models is approximately 2.0 times the energy dissipation of the reference model. For these specimens as the reinforcement ratio of coupling beams increases the amount of dissipated energy decreases gradually. Again, the energy dissipation of models with shear coupling beams is lower than that for the flexural coupling beams.

5- Conclusion

One of the major problems of the coupled shear wall systems is the early collapse of coupling beams in shear mode. In this research, the effects of changing the failure mode of the coupling beams were investigated by dividing the deep connector beams into two shallow flexural beams. For this purpose, a tested coupled shear wall available in the literature was modeled numerically and modeling techniques were assessed against experimental data. Results of the analysis on twenty-six finite element models were employed to investigate the effects of using divided coupling beams with different reinforcement ratios, beam heights, and the number of stories. Based on the results:

- Dividing the shear wall coupling beams increases the ductility level of the lateral load resisting system while it may cause a reduction in the overall stiffness and strength of the entire assembly.
- Stiffness and strength reduction in coupled shear walls with divided beams may be compensated by providing additional reinforcement.
- Divided coupling beams prevent brittle failure by changing the failure mechanism from shear failure to flexural mechanism characterized by the formation of plastic hinges

at the ends of coupling beams.

- Degradation of wall piers in models with divided coupling beams starts at higher drift ratios, compared to the models with a single coupling beam at each level.
- Higher levels of energy dissipation rate and seismic ductility may be achievable together with adequate stiffness and strength, utilizing divided coupling beams with optimum ratios of longitudinal reinforcement.

It is worthy to note, although the results of the numerical analysis showed that the proposed idea may improve the seismic behavior of the system by changing the failure mechanism of coupling beams, but its application in real structural systems needs further experimental and numerical studies concerning different characteristics of these lateral load resisting systems. Also, a more rational comparison between different models can be carried out by evaluating the seismic response of some building models having different types of shear walls subjected to dynamic analysis.

References

[1] N.S. Vu, B. Li, K. Beyer, Effective stiffness of reinforced concrete coupling beams, Engineering Structures, 76 (2014) 371-382.

[2] T. Paulay, The displacement capacity of reinforced concrete coupled walls, Engineering Structures, 24(9) (2002) 1165-1175.

[3] S. Meftah, A. Tounsi, E. Adda-Bedia, Dynamic behavior of stiffened and damaged coupled shear walls, Computers and Concrete, 3(5) (2006) 285-299.

[4] B. Doran, Elastic-plastic analysis of R/C coupled shear walls: The equivalent stiffness ratio of the tie elements, Journal of the Indian Institute of Science, 83(3&4) (2003) 87.

[5] K. Bozdogan, A method for free vibration analysis of stiffened multi-bay coupled shear walls, Asian journal of civil engineering (building and housing), 7(6) (2006) 639-649.

[6] J. Hoenderkamp, The influence of single shear walls on the behavior of coupled shear walls in high-rise structures, Procedia Engineering, 14 (2011) 1816-1824.

[7] A.A. Eljadei, K.A. Harries, Design of coupled wall structures as evolving structural systems, Engineering Structures, 73 (2014) 100-113.

[8] C.C. Hung, Y.F. Su, On modeling coupling beams incorporating strain-hardening cement-based composites, Computers and Concrete, 12(4) (2013) 565-583.

[9] S. Gwon, M. Shin, B. Pimentel, D. Lee, Nonlinear modeling parameters of RC coupling beams in a coupled wall system, Earthquakes and Structures, 7(5) (2014) 817-842.

[10] M. Hajsadeghi, T. Zirakian, A. Keyhani, R. Naderi, A. Shahmohammadi, Energy dissipation characteristics of steel coupling beams with corrugated webs, Journal of Constructional Steel Research, 101 (2014) 124-132.

[11] S.W. Han, C.S. Lee, M. Shin, K. Lee, Cyclic performance of precast coupling beams with bundled diagonal reinforcement, Engineering Structures, 93 (2015) 142-151.

[12] X. Liang, P. Xing, Seismic behavior of fiber reinforced cementitious composites coupling beams with conventional reinforcement, Earthquakes and Structures, 14(3) (2018) 261-271.

[13] P. Pan, Y. Cao, H. Wang, J. Sun, Development of double-stage yielding coupling beam damper, Journal of Constructional Steel Research, 172 (2020) 106147.

[14] W. Hou, G. Lin, B. Chen, Z. Guo, Cyclic behavior and analysis of steel plate reinforced concrete coupling beams with a span-to-depth ratio of 2.5, Soil Dynamics and Earthquake Engineering, 148 (2021) 106817.

[15] K.A. Soudki, T.G. Sherwood, Behaviour of reinforced concrete beams strengthened with carbon fibre reinforced polymer laminates subjected to corrosion damage, Canadian journal of civil engineering, 27(5) (2000) 1005-1010.

[16] Z. Zhao, A. Kwan, Nonlinear behavior of deep reinforced concrete coupling beams, Structural Engineering and Mechanics, 15(2) (2003) 181-198.

[17] R. Taleb, H. Bechtoula, M. Sakashita, N. Bourahla, S. Kono, Investigation of the shear behavior of multi-story reinforced concrete walls with eccentric openings, Computers & Concrete, 10(4) (2012) 361-377.

[18] Z. Zhao, A. Kwan, X. He, Nonlinear finite element analysis of deep reinforced concrete coupling beams, Engineering Structures, 26(1) (2004) 13-25.

[19] Y. Choi, P. Hajyalikhani, S.-H. Chao, Seismic Performance of Innovative Reinforced Concrete Coupling Beam--Double-Beam Coupling Beam, ACI Structural Journal, 115(1) (2018) 113-125.

[20] C. Chen, Q. Zeng, Z. Gao, L. Sui, Y. Zhou, FRP-Reinforced Concrete–Steel Double-Skin Tubular Coupling Beam Subjected to Reversed Cyclic Loading, Journal of Composites for Construction, 25(4) (2021) 04021033.

[21] L. Sui, Y. Liu, Z. Zhu, B. Hu, C. Chen, Y. Zhou, Seismic Performance of LRS-FRP–Concrete–Steel Tubular Double Coupling Beam, Applied Sciences, 11(5) (2021) 2024.

[22] R. Liu, M. Wang, X. Chen, W. Zhu, J. Fu, Experimental analysis on seismic behavior of small-span-to-depth-ratio slotted coupling beams with slab and HRB500 bar, Journal of Civil, Architectural & Environmental Engineering (JCAEE), 38 (2016) 9-16 (Chinese).

[23] X. Li, Y.-S. Sun, B.-D. Ding, C.-Z. Xia, Cyclic Behavior of Deep RC Coupling Beams with Different Reinforcement Layouts, Journal of Earthquake Engineering, 24(1) (2018) 1-20.

[24] M. Li, J.G. Chen, W.J. Zhao, L.G. Wang, Force behavior of parallel double coupling beams with different widths, Applied Mechanics and Materials, Vols. 578-579 (2014) 707-710.

[25] M. Li, H. Zhang, Y. Wang, W. Tao, B. Wang, R. Shan, Analysis of the Influencing Factors on the Load-deformation Skeleton Curves of PDCB, in: 2015 International Conference on Mechatronics, Electronic, Industrial and Control Engineering (MEIC-15), Atlantis Press, 2015.

[26] D. Yu, C. Wang, Restoring force model of semi seam coupling beam based on ABAQUS, World Information on Earthquake Engineering, 33 (2017) 89-96 (Chinese).

[27] J. Chen, L. Liu, J. Zou, Study on seismic performance of coupling beams between cast-in-situ and prefabricated frame shear wall, in: 2017 3rd International Forum on Energy, Environment Science and Materials (IFEESM 2017), Atlantis Press, 2018.

[28] J. Chen, Study on the Force Behavior of Parallel Double Precast Coupling Beams with Different Width, in: IOP Conference Series: Earth and Environmental Science, IOP Publishing, 2019, pp. 032079.

[29] D. Yu, Z. Xu, C. Wang, Analysis of seismic behavior of shear wall structures with semi seam coupling beams, World Information on Earthquake Engineering, 33 (2017) 78-86.

[30] ACI-318, Building code requirements for structural concrete and commentary, in, American Concrete Institute, 2014.

[31] B. Broadhouse, The Winfrith concrete model in LS-DYNA3D. SPD/D (95)363, Structural performance department, Atomic Energy Authority (AEA) Technology, Winfrith Technology Center, SPD/D (95)363, 1995.

[32] B. Broadhouse, DRASTIC: A Computer Code for Dynamic Analysis of Stress Transients in Reinforced Concrete, UKAEA Atomic Energy Establishment, 1986.

[33] S. Epackachi, A.S. Whittaker, A.H. Varma, E.G. Kurt, Finite element modeling of steel-plate concrete composite wall piers, Engineering Structures, 100 (2015) 369-384.

[34] J.O. Hallquist, LS-DYNA Keyword User's Manual, vol. I, Livermore Software Technology Corporation (LSTC), (2013).

[35] J.O. Hallquist, LS-DYNA Keyword User's Manual, vol. II, Livermore Software Technology Corporation (LSTC), (2013).

[36] A. Ali, J.K. Wight, RC structural walls with staggered door openings, Journal of Structural Engineering, 117(5) (1991) 1514-1531.

[37] X. Lu, Y. Chen, Modeling of coupled shear walls and its experimental verification, Journal of Structural Engineering, 131(1) (2005) 75-84.

[38] S. Ghosh, D. Datta, A.A. Katakdhond, Estimation of the Park–Ang damage index for planar multi-storey frames using equivalent single-degree systems, Engineering Structures, 33(9) (2011) 2509-2524.

HOW TO CITE THIS ARTICLE

A. Gholizad , S. Teymour-Moghaddam, V. Akrami, Seismic Evaluation of Coupled Shear Walls with Divided Coupling Beams , AUT J. Civil Eng., 5(2) (2021) 325-338.

DOI: 10.22060/ajce.2021.19849.5750

This page intentionally left blank